Enhanced Electron–Electron Entanglement in Few-Cycle Laser-Atom Interactions

Jingyu Zhang[1], Zhifeng Cao[1], Xiaolei Hao[1*], Weidong Li[2], and Jing Chen[3,4*]

[1]*Institute of Theoretical Physics and Department of Physics, State Key Laboratory of Quantum Optics and Quantum Optics Devices, Collaborative Innovation Center of Extreme Optics, Shanxi University, Taiyuan 030006, China*
[2]*Shenzhen Key Laboratory of Ultraintense Laser and Advanced Material Technology, and College of Engineering Physics, Shenzhen Technology University, Shenzhen 518118, China*
[3]*Department of Modern Physics, and Hefei National Research Center for Physical Sciences at the Microscale and School of Physical Sciences, University of Science and Technology of China, Hefei 230026, China*
[4]*Hefei National Laboratory, Hefei 230088, China*

(Received 18 June 2025; accepted manuscript online 5 September 2025)

The rapid advancements of ultrafast intense laser technology have opened new avenues for investigating entanglement in laser-induced systems. However, the application of these advances in quantum technology requires a reliable and universally applicable method for enhancing and regulating entanglement. Here we demonstrate how a few-cycle intense laser field can significantly enhance the degree of entanglement compared to its multi-cycle counterpart, using the example of electron–electron entanglement of orbital angular momentum (OAM) states in recollision-excitation non-sequential double ionization of Ar atoms. By confining the ionization dynamics to a specific narrow time window, the few-cycle pulse purifies the electron trajectories, thereby ensuring high coherence between entangled OAM channels and enhancing entanglement. Furthermore, the degree of entanglement can be efficiently modulated by varying the carrier envelope phase of the few-cycle laser pulse, which is achieved by altering the population across OAM channels. Optimizing coherence through electron trajectory purification with a designed specific temporal waveform of laser field provides a general pathway for enhancing entanglement in laser-induced systems.

DOI: 10.1088/0256-307X/42/11/110301 CSTR: 32039.14.0256-307X.42.11.110301

1. Introduction. Ultrafast intense laser fields, characterized by their extremely short widths and high peak intensities, offer a powerful tool for probing electron dynamics on their natural timescales. Recent experimental advancements in femtosecond and attosecond laser technology have inspired researchers to explore the manifold novel aspects of ultrafast physics.[1–5] Among these, the phenomenon of quantum entanglement during the interaction between ultrashort laser pulses and atoms or molecules stands out as a particularly intriguing and promising area in recent years.[5] These investigations encompass a range of topics, including photon entanglement in high-harmonic generation,[6–8] photoelectron-ion[9–14] and atom–atom entanglement[15] in laser-induced ionization and dissociation, as well as electron–electron entanglement[16,17] in laser-induced nonsequential double ionization (NSDI) of atoms.

Among these ultrafast processes, the NSDI process is regarded as a dramatic manifestation of electron–electron correlation in nature. The rich correlated electron dynamics in the NSDI process have been extensively investigated, leading to the observation of numerous intriguing phenomena.[18–20] These include various electron correlations with different characteristics,[21–24] the transitions between them,[23,25] and quantum interference in forming them.[26,27] The observed correlations can be attributed primarily to laser-induced electron–electron collisions,[28–33] which can be regarded as a form of classical correlation. The issue of whether quantum correlation, i.e., quantum entanglement, exists between two photoelectrons remains unresolved despite recent theoretical advancements.[16] However, the precise relationship between entanglement in such systems and the underlying electron dynamics remains insufficiently understood. Moreover, whether entanglement can be effectively enhanced through modulation of electron motion warrants further exploration.

The development of quantum entanglement in ultrafast physics may offer promising alternative resources for quantum technology,[34] particularly the potential for entanglement to enhance attosecond imaging processes.[16] The translation of these advances in ultrafast physics into quantum technology, however, remains challenging at present. A significant impediment pertains to the degree of entanglement. It is widely acknowledged that the application of quantum entanglement in quantum information[35] and quantum metrology[36,37] requires a high degree of entanglement. However, even at the theoretical level,

*Corresponding authors. Email: xlhao@sxu.edu.cn; chenjing@ustc.edu.cn
© 2025 Chinese Physical Society and IOP Publishing Ltd. All rights, including for text and data mining, AI training, and similar technologies, are reserved.

the degree of entanglement predicted for NSDI in noble gas systems—currently the most experimentally accessible platform—remains relatively low.[16] In the domain of traditional quantum information, there has been significant progress in developing effective modulation and enhancement techniques for entanglement, including enhancing macroscopic mechanical entanglement in integrated optics and cavity optomechanics,[38–42] as well as establishing quantum error correction and entanglement distillation schemes for quantum information processing and communication.[43–45] Similarly, a reliable and universally applicable method for enhancing and regulating entanglement in ultrafast physics is also required.

The degree of entanglement is typically determined by the population and coherence intensity of particles in different states involved in the entanglement, and this, in turn, indicates the common manner in which the degree of entanglement may be modified by altering the population or coherence, or a combination of both. The ultrashort laser technology, recognized for its capacity to regulate time-domain waveforms of laser fields, has exhibited its ability to precisely manipulate the motion of electrons, consequently regulating the population[46–48] and coherence[12,49–51] of the states involved in various coherent processes within few-body systems. This strongly implies the feasibility of entanglement modulation through the utilization of ultrashort pulses.

In this work, we develop a modified Coulomb-corrected quantum trajectories (CCQT) method[33,52] in a vortex wave picture[53] and demonstrate a universal technical pathway to enhance and regulate entanglement in ultrafast physics. This is achieved by controlling the time-domain waveform of the laser field, thereby regulating electron dynamics, and ultimately controlling the population and coherence of quantum states in the system, achieving control over the degree of entanglement. We will use the example of electron–electron entanglement of orbital angular momentum (OAM) states in NSDI of atoms to illustrate how a few-cycle intense laser field can effectively improve the coherence between different ionization channels of the entangled electrons, thereby tripling the degree of entanglement compared to its multi-cycle counterpart. Moreover, the population on different OAM states can be modulated by varying the carrier envelope phase (CEP) of the few-cycle laser pulse, which can be freely adjusted under present experimental conditions. This results in an evident modulation of the degree of entanglement with CEP.

2. Methods. The entanglement of two photoelectrons generated through the highly correlated NSDI process has been studied in multi-cycle pulses using the strong-field approximation (SFA),[16] in which the Coulomb interaction between the photoelectrons and the residual ions is neglected. The SFA predicts a relatively low degree of entanglement for noble gases, which are experimentally accessible for coincidence measurements. Numerous studies have shown that the Coulomb potential plays an important role in the ionization dynamics of atoms and molecules in ultrafast laser fields.[54–58] In order to accurately account for electron–electron correlations and to clearly explore the connection between entanglement and electron dynamics, we employ a modified CCQT method in a vortex wave framework, which incorporates both quantum effects and Coulomb interactions between the residual ion and ionized electrons into a uniform theory.[33,52] The CCQT method has been successfully applied to quantitatively reproduce the experimentally observed cross-shaped and anti-correlated patterns of correlated electron momentum distribution, as well as transitions between them.[59–61] Besides this, the application of CCQT method allows us to identify the influence of Coulomb potential on entanglement.

The NSDI process follows a three-step mechanism.[18,28] Initially, one electron (e_1) is tunneling ionized from the atomic ground state. It then experiences a laser-driven recollision with the parent ion, transferring energy to the bound electron (e_2). Finally, e_2 can be ionized directly [recollision-impact ionization (RII)] or only pumped to an excited state and subsequently ionized [recollision-excitation-with-subsequent-ionization (RESI)] by the laser field to the two-electron continuum state. In the RESI pathway, e_2 may be excited to different OAM states upon recollision. The RESI process, as depicted in Figs. 1(a) and 1(b), will be discussed in detail later on. In this context, the quantum observable of the free electron's OAM is defined with respect to the polarization direction of the external laser field and characterizes the vortex nature of the electron's wavefunction. Currently, a host of techniques are available to measure the OAM of electron beams.[53,62–64] As the process under consideration is rotationally symmetric around the polarization axis of the linearly polarized laser field, there are two angular momentum conservation laws in this direction: (i) the total angular momentum of the two-electron system is conserved throughout the entire process, meaning that the sum of magnetic quantum numbers in the initial ground state equals the combined azimuthal OAM carried by the two electrons in the ionized continuum state, $m_1+m_2=l_1+l_2$; and (ii) the angular momentum of e_2 is conserved from the intermediate excited state to the final continuum state, $m_e=l_2$. The corresponding derivation is provided in Eq. (S15) of the Supplementary Materials (SM). The fact that the OAMs of two electrons are determined by their excitation channels of e_2 implies that the final two-electron state, expressed as an entangled superposition of OAM states, can be analyzed through coherence between these different excitation channels. If only the magnetic quantum numbers of ground states of e_1 and e_2 with $m_1=m_2=0$, as well as the excited state of e_2 with $m_e=0,\pm1$ are taken into account, which dominate the process,[16] the final two-electron continuum state can thus be expanded in the OAM basis $|l_1,l_2\rangle$ as follows:

$$\begin{aligned}|\Psi(\tilde{\boldsymbol{p}}_1,\tilde{\boldsymbol{p}}_2)\rangle &= M_{0,0}(\tilde{\boldsymbol{p}}_1,\tilde{\boldsymbol{p}}_2)|0,0\rangle + M_{1,-1}(\tilde{\boldsymbol{p}}_1,\tilde{\boldsymbol{p}}_2)|1,-1\rangle \\ &\quad + M_{-1,1}(\tilde{\boldsymbol{p}}_1,\tilde{\boldsymbol{p}}_2)|-1,1\rangle . \end{aligned} \tag{1}$$

Here $\tilde{\boldsymbol{p}}_i$ denotes the Coulomb field-disturbed 2D final momentum of two electrons with the azimuth integrated out,

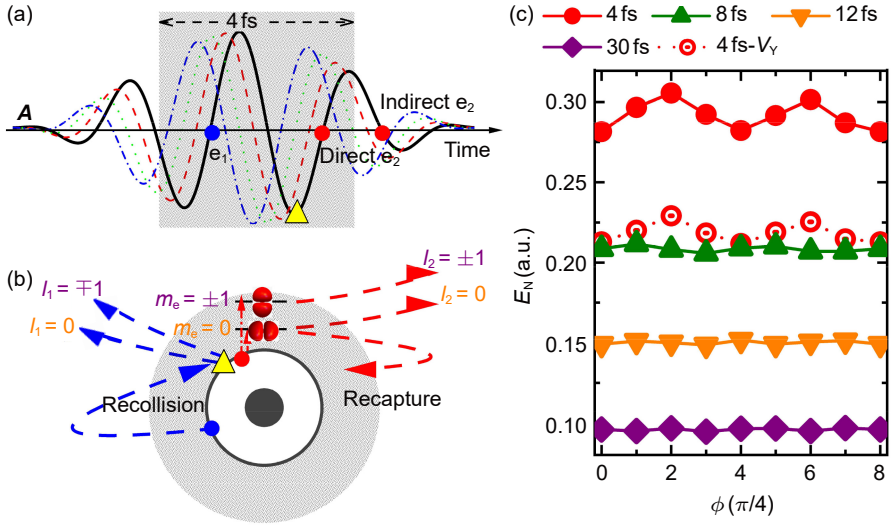

Fig. 1. (a) Laser vector potential $\boldsymbol{A}$ for a 4 fs pulse with various CEPs, where $\phi = 0, \pi/4, \pi/2$, and $3\pi/4$ are donated by solid, dashed, dotted, and dash-dotted lines, respectively. Each recolliding electron (e_1, indicated by the blue dot) has the potential to trigger both direct and indirect ionization of the second electron (e_2, indicated by the red dots), typically occurring around 1 and 1.5 optical cycles following its tunneling ionization. Their recollision is marked by a yellow triangle. (b) RESI process described in the text; due to the recollision of e_1, e_2 can be pumped to excited states with different magnetic quantum numbers m_e, leading to distinct final OAM states of two electrons. The two types of OAM channels are indicated by the purple and orange labels. Ionization from the $m_e = 0$ channel—whose electronic cloud is aligned along the laser polarization direction—is more susceptible to recapture by the parent ion. (c) The degree of entanglement (E_N) over CEPs with different pulse widths. The results denoted as 4fs-V_Y are obtained by replacing the Coulomb potential with the Yukawa potential for 4 fs.

i.e., $\tilde{\boldsymbol{p}}_i = (\tilde{p}_{iz}, \tilde{p}_{i\perp})$, where $\tilde{p}_{iz}$ and $\tilde{p}_{i\perp}$ represent the momentum components along and perpendicular to the polarization direction of the laser field, respectively. Due to the indistinguishability of the two electrons, the states $|1,-1\rangle$ and $|-1,1\rangle$ are physically equivalent.

The transition amplitudes $M_{l_1,l_2}(\tilde{\boldsymbol{p}}_1, \tilde{\boldsymbol{p}}_2)$ for the two channels $|0,0\rangle$ and $|1,-1\rangle$ simulated with the modified CCQT method in the vortex wave picture can be expressed as [see Eqs. (S33) and (S34) of the SM for more details]

$$M_{0,0}(\tilde{\boldsymbol{p}}_1, \tilde{\boldsymbol{p}}_2) = 2\sum_s \left(\tilde{p}_{1z} - \tilde{k}_{sz}\right)[p_{2z} + A(t_s)] \cdot F_{\tilde{\boldsymbol{p}}_1,\tilde{\boldsymbol{p}}_2}(\tilde{\boldsymbol{k}}_s, t_s, t'_s, t''_s), \quad (2)$$

$$M_{1,-1}(\tilde{\boldsymbol{p}}_1, \tilde{\boldsymbol{p}}_2) = \sum_s \tilde{p}_{1\perp} p_{2\perp} F_{\tilde{\boldsymbol{p}}_1,\tilde{\boldsymbol{p}}_2}(\tilde{\boldsymbol{k}}_s, t_s, t'_s, t''_s). \quad (3)$$

To highlight the differences in transition amplitudes between the two channels, we consolidate all common factors into a unified function $F_{\tilde{\boldsymbol{p}}_1,\tilde{\boldsymbol{p}}_2}(\tilde{\boldsymbol{k}}_s, t_s, t'_s, t''_s)$. This function incorporates identical dynamical contributions, including the phase term $\exp(\mathrm{i}S(t_s, t'_s, t''_s))$, as well as common elements from the prefactors $V^{\#}_{\tilde{\boldsymbol{p}}_1 e,\tilde{\boldsymbol{k}}_s g}(t'_s)$ and $V^{\#}_{\boldsymbol{p}_2,e}(t''_s)$. Here, t''_s is the ionization time of e_1, $\tilde{\boldsymbol{k}}_s$ denotes its Coulomb field-disturbed asymptotic momenta prior to collision, t'_s is the recollision time, and t_s corresponds to the ionization time of e_2 from the excited state. The two formulas demonstrate that the $|0,0\rangle$ channel, Eq. (2), depends on the longitudinal momenta, specifically the longitudinal momentum transfer of e_1 to e_2 during recollision, $\tilde{p}_{1z} - \tilde{k}_{sz}$, and the longitudinal mechanical momentum of e_2 at the time of tunneling, $p_{2z} + A(t_s)$, where p_{2z} is the longitudinal asymptotic momentum and $A(t_s)$ is the laser field vector potential. In contrast, the $|1,-1\rangle$ channel, Eq. (3), depends on the transverse momenta, which include the transverse momentum of e_1 following recollision, $\tilde{p}_{1\perp}$, and the transverse momentum of e_2 at the time of tunneling, $p_{2\perp}$. It should be noted that $p_{2z} + A(t_s)$ is purely imaginary, as it satisfies the saddle-point equation for tunneling: $[p_{2z} + A(t_s)]^2/2 + p_{2\perp}^2/2 = -I_{\mathrm{pe}}$, where I_{pe} is the binding potential. The discrepancy between the two channels can be attributed to the distinct spatial distributions of the respective excited state wave functions from which e_2 is emitted, see Fig. 1(b). In the case of the excited state with $m_e = 0$, which corresponds to the $|0,0\rangle$ channel, the wave function exhibits a distribution along the polarization axis. Conversely, in the case of the excited state with $m_e = \pm 1$, which corresponds to the $|1,-1\rangle$ channel, the wave function displays a distribution perpendicular to the polarization axis.

In order to quantify the entanglement between two photoelectrons, the logarithmic negativity (E_N) criterion [65,66] is employed. Compared to alternative measures such as purity or von Neumann entropy, E_N is preferred in this context for two principal reasons: (i) it effectively quantifies entanglement in mixed states, a critical feature for analyzing entanglement in future experiments; and (ii) it offers a well-defined operational interpretation, thereby providing clear insight into the origin and nature of entanglement in electron pairs generated via RESI. After tracing over all the continuous momentum components, E_N can be reduced in the context of the OAM basis [62,63,67] (see SM

Part II for more details),

$$E_{\mathrm{N}} = \log_2\left(1 + 2\alpha_{1,1} + 4\left|\alpha_{0,1}\right|\right), \tag{4}$$

where

$$\alpha_{1,1} = \int\int \mathrm{d}^2\tilde{\boldsymbol{p}}_1 \mathrm{d}^2\tilde{\boldsymbol{p}}_2 \left|M_{1,-1}\left(\tilde{\boldsymbol{p}}_1, \tilde{\boldsymbol{p}}_2\right)\right|^2, \tag{5}$$

represents the population of the $|1,-1\rangle$ channel, and

$$\alpha_{0,1} = \int\int \mathrm{d}^2\tilde{\boldsymbol{p}}_1 \mathrm{d}^2\tilde{\boldsymbol{p}}_2 \left|M_{0,0}\left(\tilde{\boldsymbol{p}}_1, \tilde{\boldsymbol{p}}_2\right)\right| \left|M_{1,-1}\left(\tilde{\boldsymbol{p}}_1, \tilde{\boldsymbol{p}}_2\right)\right| \cdot \exp(\mathrm{i}\left[\Phi_{0,0}\left(\tilde{\boldsymbol{p}}_1, \tilde{\boldsymbol{p}}_2\right) - \Phi_{1,-1}\left(\tilde{\boldsymbol{p}}_1, \tilde{\boldsymbol{p}}_2\right)\right]), \tag{6}$$

denotes the coherence between channels $|0,0\rangle$ and $|1,-1\rangle$, which depends on both the populations of the two channels and the degree of phase matching between them. Here, the modulus and phase associated with a given channel $|l_1, l_2\rangle$ are represented by $\left|M_{l_1,l_2}\left(\tilde{\boldsymbol{p}}_1, \tilde{\boldsymbol{p}}_2\right)\right|$ and $\Phi_{l_1,l_2}\left(\tilde{\boldsymbol{p}}_1, \tilde{\boldsymbol{p}}_2\right)$, respectively. The degree of phase matching, defined as the phase difference $\Phi_{0,0}\left(\tilde{\boldsymbol{p}}_1, \tilde{\boldsymbol{p}}_2\right) - \Phi_{1,-1}\left(\tilde{\boldsymbol{p}}_1, \tilde{\boldsymbol{p}}_2\right)$, reflects the concentration of this phase difference across momentum space. This indicates that a constant phase difference distribution, corresponding to the maximum degree of phase matching, can be factored out of the momentum integral, thereby yielding the greatest contribution to the coherent intensity $\alpha_{0,1}$. A value of $E_{\mathrm{N}} = 0$ indicates a completely separable (non-entangled) state, while larger values correspond to higher degrees of entanglement. The system reaches its maximum entangled state, characterized by $E_{\mathrm{N}} = 1.58$, when the population of $|1,-1\rangle$ channel is twice that of $|0,0\rangle$ channel, and the distribution of phase difference between the two channels remains constant across the entire momentum space. In our calculations, the populations of different OAM channels are normalized. Consequently, the degree of entanglement can be controlled by regulating the populations of the two channels and the coherence between them.

3. Results and Discussion. Figure 1(c) displays the simulated degree of entanglement between two photoelectrons ionized via the RESI process, where the logarithmic negativity E_{N} is presented as a function of the laser pulse's CEP for various pulse widths. The laser pulse is linearly polarized, described by the formula $\boldsymbol{A}(t) = A_0 \sin^2(1.14t/\tau_p)\cos(\omega t + \phi)\,\boldsymbol{e}_z$, with a center wavelength of 800 nm and intensity of $1.1 \times 10^{14}\,\mathrm{W/cm^2}$. The pulse width τ_{p} is defined as the full width at half maximum of the intensity, and the CEP ϕ ranges from 0 to 2π. The laser vector potentials for a 4 fs pulse with various CEPs are depicted in Fig. 1(a). All electron dynamics illustrated in Figs. 1(a) and 1(b) impact the coherence of the two OAM channels, ultimately affecting the degree of entanglement between the two electrons.

As illustrated in Fig. 1(c), a significant increase in entanglement is observed with a decrease in pulse width. In particular, the value of E_{N} increases threefold when the pulse width is decreased from 30 fs to 4 fs. Furthermore, the degree of entanglement can be modulated by varying the CEP of the 4 fs few-cycle pulse, with an amplitude of up to 10%. However, for the pulse widths of 8 fs, 12 fs, and 30 fs, the entanglement remains almost unchanged with CEP. Additionally, the results obtained by replacing the Coulomb potential with the short-range Yukawa potential in the calculation are presented in order to identify the influence of the Coulomb potential. Figure 1(c) indicates that the entanglement is significantly elevated under the Coulomb potential compared to the Yukawa potential.

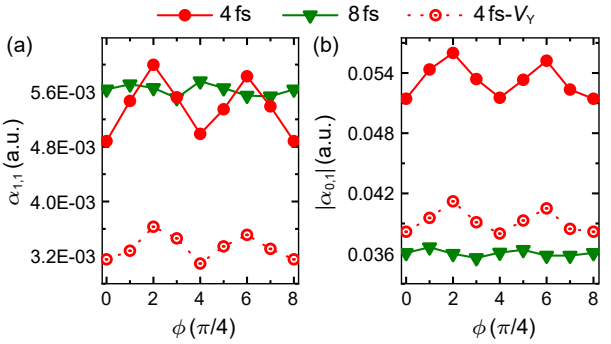

Fig. 2. (a) The population of the $|1,-1\rangle$ channel ($\alpha_{1,1}$). (b) The coherence between channels $|0,0\rangle$ and $|1,-1\rangle$ ($|\alpha_{0,1}|$) over CEPs with different pulse widths. Symbols and line styles follow the same conventions as in Fig. 1(c).

Taking 4 fs and 8 fs as examples, it is possible to analyze the enhancement and modulation of entanglement through the population of the $|1,-1\rangle$ channel, $\alpha_{1,1}$, as illustrated in Fig. 2(a), and the coherence intensity $\alpha_{0,1}$, as shown in Fig. 2(b). It should be noted that $\alpha_{0,1}$ depends on both the degree of phase matching between the two channels and the population of each channel, according to Eq. (6).

Figure 2(a) demonstrates that the value of $\alpha_{1,1}$ for 4 fs exhibits oscillatory behavior around the CEP-independent value of $\alpha_{1,1}$ for 8 fs. This indicates that the modulation of entanglement with CEP at 4 fs is a consequence of the modulation of $\alpha_{1,1}$. However, the nearly identical CEP-averaged values for both pulse widths suggest that the significant enhancement in entanglement observed for the shorter pulse width is unrelated to $\alpha_{1,1}$. In contrast, the value of $\alpha_{0,1}$ for 4 fs is considerably higher than that for 8 fs, as shown in Fig. 2(b). It can therefore be concluded that the observed enhancement of entanglement at 4 fs can be attributed to increased coherence intensity between the two channels; in particular, the increased degree of phase matching between them. With respect to the impact of the Coulomb potential, figure 2(a) illustrates that it predominantly enhances $\alpha_{1,1}$. Subsequently, we will elucidate the mechanisms through which a 4 fs few-cycle pulse can significantly enhance the coherence intensity and the manner in which the CEP and the Coulomb potential influence the population of the $|1,-1\rangle$ channel.

3.1. The Effect of Pulse Width. The enhancement of entanglement observed in a 4 fs few-cycle pulse is a consequence of the increased coherence intensity and, in particular, the improved degree of phase matching between the two channels. To demonstrate this, we set the phase difference between the two channels to be constant across

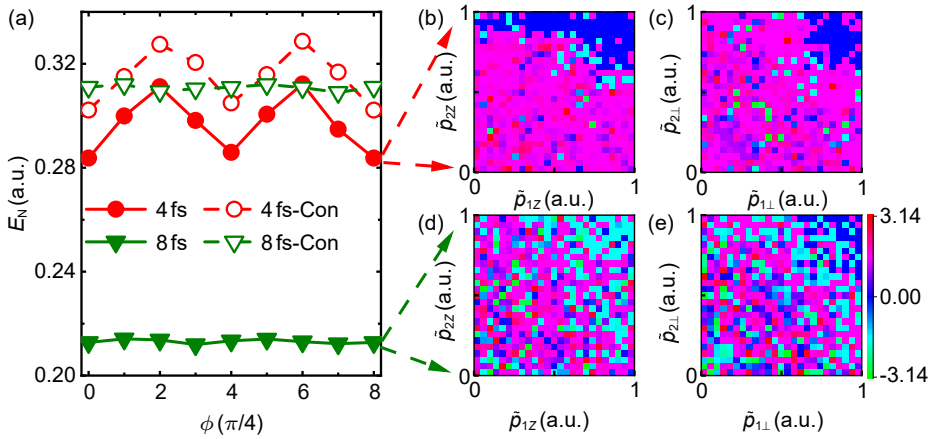

Fig. 3. (a) E_{N} over CEPs when the phase difference between the two channels is artificially set to be constant (Con). The original results in Fig. 1(c) are also presented for comparison. (b)–(e) The distributions of the phase differences between the two channels in momentum space at CEP of 0. In panels (b) and (d) of longitudinal momentum space, the transverse momenta of the two electrons are fixed at $\tilde{p}_{1\perp} = 0.18$ a.u., and $\tilde{p}_{2\perp} = 0.38$ a.u.; while in panels (c) and (e) of transverse momentum space, the longitudinal momenta are fixed at $\tilde{p}_{1Z} = \tilde{p}_{2Z} = 0.02$ a.u. These values are selected to ensure a relatively high ionization rate.

different momenta in Eq. (6), which represents the maximum degree of phase matching. It is observed that, in comparison to the original results, the degree of entanglement for a 4 fs pulse increases slightly, whereas that for an 8 fs pulse undergoes a significant enhancement, ultimately reaching the same value as that for a 4 fs pulse, as illustrated in Fig. 3(a). This supports our conclusion. The distributions of phase difference between the two channels in momentum space are presented in Figs. 3(b)–3(e) to illustrate the degree of phase matching at two pulse widths. Uniform distributions are observed at 4 fs, while chaotic distributions are observed at 8 fs. This indicates that the phase difference between the two channels is almost constant for 4 fs, but not for 8 fs.

The phase difference between the two channels can be clearly derived by comparing Eqs. (2) and (3), in which $p_{2z} + A(t_s)$ is purely imaginary while all other momentum terms are real. Therefore, the phase difference between the two channels is either $\pi/2$ or $-\pi/2$, depending on the sign of $p_{2z} + A(t_s)$. As is well known for e_2, in the process of tunneling ionization, two distinct trajectories are generated in each optical cycle. These are known as the direct and indirect trajectories [denoted by two red points in Fig. 1(a)], and they possess the same final momentum. The momenta $p_{2z} + A(t_s)$ of these two trajectories are of opposite signs. In the case of a multi-cycle laser pulse, both trajectories contribute significantly, resulting in a chaotic phase difference between the two channels. Furthermore, the coherent superposition of direct trajectories (with phase difference $\pi/2$ in this text) and indirect trajectories (with phase difference $-\pi/2$) results in an even more irregular phase difference distribution, as clearly observed in Figs. 3(d) and 3(e). Whereas in the case of a few-cycle pulse [e.g., the 4 fs pulse in Fig. 1(a)], the ionization of e_2 predominantly occurs at the falling edge of the pulse [the left red point in Fig. 1(a)]. The indirect trajectory [the right red point in Fig. 1(a)], which emerges later, experiences a substantially weaker electric field compared to the direct trajectory, leading to a substantial suppression of its contribution. This indicates that the electron trajectories have been effectively purified. The presence of the sole direct trajectories gives rise to a phase difference distribution that is uniformly concentrated at the value of $\pi/2$ for 4 fs, as observed in Figs. 3(b) and 3(c). Consequently, the temporal confinement imposed by few-cycle laser fields facilitates trajectory purification through the suppression of indirect trajectories. This purification effect first enables near-perfect phase matching between the channels with a fixed $\pi/2$ phase difference in the 4 fs case, and further results in a marked enhancement of electron entanglement compared to multi-cycle pulses.

3.2. The Effect of CEP. Comparing Fig. 2(a) with Fig. 1(c), $\alpha_{1,1}$ at 4 fs shows synchronized oscillation with E_{N}. Moreover, modifying the degree of phase matching between the two channels does not affect the oscillation behavior of E_{N}, as shown in Fig. 3(a). All these suggest that the modulation of entanglement with CEP at 4 fs is due to the modulation of the population of the $|1,-1\rangle$ channel. Our analysis indicates that the population of $|0,0\rangle$ channel is directly influenced by the CEP. As the overall probability is normalized, this is equivalent to modulating the population of the $|1,-1\rangle$ channel. According to Eq. (2), the population of the $|0,0\rangle$ channel depends on the longitudinal momentum transfer, $\tilde{p}_{1z} - \tilde{k}_{sz}$. A change in the CEP results in a corresponding alteration in the temporal waveform of the laser field, which in turn affects $\tilde{k}_{sz}$, the momentum of the returning e_1. This leads to a change in the momentum transfer during the inelastic scattering process. The larger amplitude of vector potential at the recollision time [see the yellow triangle in Fig. 1(a)], the greater collision energy and thus the smaller momentum transfer. Ultimately the population of the $|0,0\rangle$ channel is decreased. Figure 4(a) illustrates the distribution of momentum transfer at various CEPs. Upon changing the CEP from 0 to $\pi/2$, the distribution exhibits a slight shift towards lower momentum. This indicates a reduction

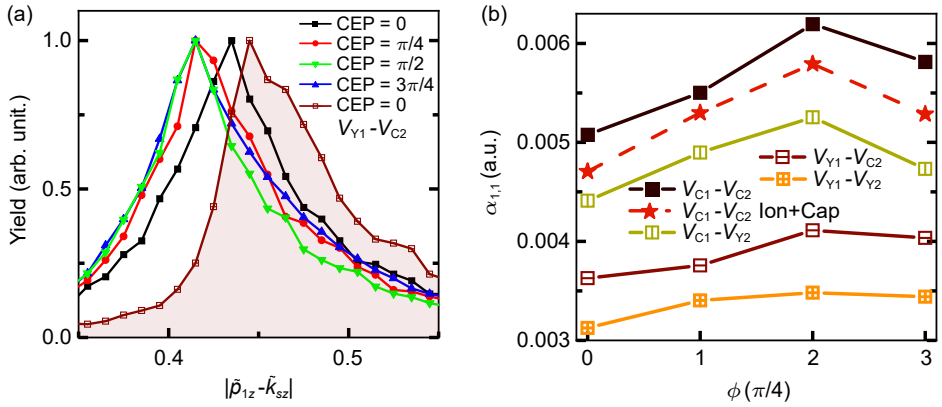

Fig. 4. (a) The distributions of the longitudinal momentum transfer during the recollision of e_1 in the $|0,0\rangle$ channel at different CEPs of a 4 fs laser pulse. The distribution in the case that e_1 experiences a Yukawa potential (V_Y) while e_2 experiences a Coulomb potential (V_C) at a CEP of 0, denoted as V_{Y1}–V_{C2}, is also presented by a curve with shading. Each curve is normalized through the process of division by the maximum value. (b) $\alpha_{1,1}$ over CEPs in the cases where e_1 is either under V_C or under V_Y, while e_2 also has two choices, generating four combinations, denoted as V_{C1}–V_{C2}, V_{Y1}–V_{C2}, V_{C1}–V_{Y2}, and V_{Y1}–V_{Y2} (solid line). The results including both ionized and captured e_2, denoted as V_{C1}-V_{C2} Ion+Cap are also presented (dashed line).

in the population of the $|0,0\rangle$ channel, while the population of the $|1,-1\rangle$ channel increases. This is consistent with the observed changes in $\alpha_{1,1}$ [see Fig. 2(a)]. A similar effect of CEP on the electron–electron entanglement has been reported recently within the framework of time-dependent Schrödinger equation method in continuous coordinate and momentum space.[17] They demonstrated that the entanglement primarily emerges during the period when electrons collide with each other.

3.3. The Effect of Coulomb Potential. The Coulomb potential primarily influences two processes within our calculations: (i) the evolution of e_1 between the tunneling ionization and the recollision, and (ii) the evolution of e_2 following its tunneling ionization. In order to ascertain why the populations of the two channels are different in a Coulomb potential (V_C) and a short-range Yukawa potential (V_Y), we dissect the effects on e_1 and e_2 separately. We consider scenarios where e_1 is either under V_C or under V_Y, while e_2 also has two choices. There are ultimately four combinations, which are all presented in Fig. 4(b). A comparison of the four cases reveals that both the effects of the Coulomb potential on e_1 and e_2 contribute to an increase in the entanglement degree, with the former exhibiting a more pronounced effect.

The principal effect of V_C on e_1 is to increase the momentum before recollision and reduce the momentum transfer compared to V_Y. This is confirmed by the observation that the distribution of momentum transfer exhibits a notable shift towards high momentum when applying V_Y to e_1, as illustrated in Fig. 4(a). Consequently, utilizing the Coulomb potential results in an increase in the population of the $|1,-1\rangle$ channel and eventually an enhancement of E_N. With regard to the effect of the Coulomb potential on e_2, it primarily causes some of the ionized e_2 to be recaptured, which is known as frustrated double ionization.[68,69] In comparison to the $|0,0\rangle$ channel, electrons in the $|1,-1\rangle$ channel exhibit a higher transverse momentum [see Eqs. (2) and (3)] and are more difficult to recapture. Consequently, its relative population is increased, as only the ionization portion is included in the calculation. However, if the recaptured portion is included, E_N will notably decrease, as illustrated in Fig. 4(b).

4. Conclusion. In conclusion, we utilize the example of electron–electron entanglement in OAM states in NSDI of Ar atoms to demonstrate how the degree of entanglement can be effectively enhanced and modulated through modifying the coherence and population of the states involved in the entanglement by the use of a few-cycle intense laser field. Using a modified CCQT method, which offers a more accurate representation of electron–electron correlations, we demonstrate that the coherence—particularly the degree of phase matching between different OAM channels—can be significantly enhanced. This enhancement is achieved by purifying electron trajectories, primarily by suppressing the contribution of indirect trajectory, through the confinement of ionization dynamics within a specific narrow temporal window enabled by a few-cycle laser pulse. This results in a threefold increase in the degree of electron–electron entanglement compared to the case of a multi-cycle laser pulse.

Moreover, the population of different OAM channels can be modulated by varying the CEP of the few-cycle laser pulse, and the Coulomb potential can also exert a significant influence. By varying the CEP, the momentum transfer of e_1 during inelastic scattering, which determines the relative population of different channels, is altered. This results in an amplitude modulation of approximately 10% in the degree of entanglement. The primary effect of the Coulomb potential is to diminish the momentum transfer of e_1 and enhance the recapture of e_2. This affects the population and eventually significantly elevates the degree of entanglement compared to that with short-range Yukawa potential.

The idea of enhancing entanglement through the purification of electron trajectories with a specific waveform of the laser field has further potential for extension. It can

be extended to other laser-induced entangled systems, such as photoelectron–ion entanglement and atom–atom entanglement. The purification can be achieved by designing a specific laser field waveform using laser shaping techniques, which have been effectively employed for precise control of electron motion. This will provide accessible and easily controllable entangled resources for quantum information tasks.

Nevertheless, it is important to note that significant challenges remain in the experimental detection of electron entanglement generated via RESI. Two critical unresolved issues include: (i) the experimental discrimination between electrons originating from RESI and those from RII, where the latter typically exhibit markedly reduced or negligible entanglement; and (ii) the precise measurement of the OAM of electrons ionized in the field of ultrafast physics. One potential approach to address the first challenge is to tune the laser parameters below the threshold intensity for direct recollision-induced ionization, thus suppressing the RII channel and enhancing the dominance of RESI processes in electron population.

Acknowledgements. We thank Augusto Smerzi for discussions. This work was supported by the National Natural Science Foundation of China (Grant Nos. 12274273 and 12450402) and the Innovation Program for Quantum Science and Technology (Grant No. 2021ZD0302101).

References

[1] Brabec T and Krausz F 2000 *Rev. Mod. Phys.* **72** 545
[2] Krausz F and Ivanov M 2009 *Rev. Mod. Phys.* **81** 163
[3] Mourou G 2019 *Rev. Mod. Phys.* **91** 030501
[4] Kim H, Garg M, Mandal S, Seiffert L, Fennel T, and Goulielmakis E 2023 *Nature* **613** 662
[5] Cruz-Rodriguez L, Dey D, Freibert A, and Stammer P 2024 *Nat. Rev. Phys.* **6** 691
[6] Lewenstein M, Ciappina M F, Pisanty E, Rivera-Dean J, Stammer P, Lamprou T, and Tzallas P 2021 *Nat. Phys.* **17** 1104
[7] Stammer P, Rivera-Dean J, Lamprou T, Pisanty E, Ciappina M F, Tzallas P, and Lewenstein M 2022 *Phys. Rev. Lett.* **128** 123603
[8] Gorlach A, Tzur M E, Birk M, Krüger M, Rivera N, Cohen O, and Kaminer I 2023 *Nat. Phys.* **19** 1689
[9] Nandi S, Stenquist A, Papoulia A *et al.* 2024 *Sci. Adv* **10** eado0668
[10] Jiang W C, Zhong M C, Fang Y K, Donsa S, Březinová I, Peng L Y, and Burgdörfer J 2024 *Phys. Rev. Lett.* **133** 163201
[11] Wang J P and He F 2018 *Phys. Rev. A* **97** 043411
[12] Vrakking M J J 2021 *Phys. Rev. Lett.* **126** 113203
[13] Koll L M, Maikowski L, Drescher L, Witting T, and Vrakking M J J 2022 *Phys. Rev. Lett.* **128** 043201
[14] Vrakking M J J 2022 *J. Phys. B: At. Mol. Opt. Phys.* **55** 134001
[15] Eckart S, Trabert D, Rist J, Geyer A, Schmidt L P H, Fehre K, and Kunitski M 2023 *Sci. Adv.* **9** eabq8227
[16] Maxwell A S, Madsen L B, and Lewenstein M 2022 *Nat. Commun.* **13** 4706
[17] Younis D, Xie S, and Eberly J H 2024 arXiv:2403.09854 [physics.atom-ph]
[18] Becker W, Liu X, Ho P J, and Eberly J H 2012 *Rev. Mod. Phys.* **84** 1011
[19] Faria C F d M and Liu X 2011 *J. Mod. Optic.* **58** 1076
[20] Amini K, Biegert J, Calegari F *et al.* 2019 *Rep. Prog. Phys.* **82** 116001
[21] Weber T, Giessen H, Weckenbrock M, Urbasch G, Staudte A, Spielberger L, Jagutzki O, Mergel V, Vollmer M, and Dörner R 2000 *Nature* **405** 658
[22] Rudenko A, de Jesus V L B, Ergler T, Zrost K, Feuerstein B, Schröter C D, Moshammer R, and Ullrich J 2007 *Phys. Rev. Lett.* **99** 263003
[23] Liu Y Q, Tschuch S, Rudenko A, Dürr M, Siegel M, Morgner U, Moshammer R, and Ullrich J 2008 *Phys. Rev. Lett.* **101** 053001
[24] Bergues B, Kübel M, Johnson N G *et al.* 2012 *Nat. Commun.* **3** 813
[25] Jiang H, Mandrysz M, Sanchez A *et al.* 2023 *New J. Phys.* **25** 033002
[26] Hao X L, Chen J, Li W D, Wang B B, Wang X D, and Becker W 2014 *Phys. Rev. Lett.* **112** 073002
[27] Maxwell A S and Faria C F d M 2016 *Phys. Rev. Lett.* **116** 143001
[28] Corkum P B 1993 *Phys. Rev. Lett.* **71** 1994
[29] Ho P J, Panfili R, Haan S L, and Eberly J H 2005 *Phys. Rev. Lett.* **94** 093002
[30] Sarkadi L 2020 *J. Phys. B: At. Mol. Opt. Phys.* **53** 165401
[31] Becker A and Faisal F H M 2000 *Phys. Rev. Lett.* **84** 3546
[32] Chen S G, Jiang W C, Grundmann S, Trinter F, Schöffler M S, Jahnke T, Dörner R, Liang H, Wang M X, Peng L Y, and Gong Q H 2020 *Phys. Rev. Lett.* **124** 043201
[33] Hao X L, Bai Y X, Li C, Zhang J Y, Li W D, Yang W F, Liu M Q, and Chen J 2022 *Commun. Phys.* **5** 31
[34] Lewenstein M, Baldelli N, Bhattacharya U *et al.* 2024 arXiv:2208.14769 [quant-ph]
[35] Braunstein S L and van Loock P 2005 *Rev. Mod. Phys.* **77** 513
[36] Giovannetti V, Lloyd S, and Maccone L 2011 *Nat. Photonics* **5** 222
[37] Pezze L, Smerzi A, Oberthaler M K, Schmied R, and Treutlein P 2018 *Rev. Mod. Phys.* **90** 035005
[38] Léger Z M, Brodutch A, and Helmy A S 2018 *Phys. Rev. A* **97** 062303
[39] Peng R, Zhao C S, Yang Z, Yang J Y, and Zhou L 2023 *Phys. Rev. A* **107** 013507
[40] Amazioug M, Teklu B, and Asjad M 2023 *Sci. Rep.* **13** 3833
[41] Hu C S, Huang X R, Shen L T, Yang Z B, and Wu H Z 2017 *Eur. Phys. J. D* **71** 24
[42] Zheng S S, Sun F X, Yuan H Y, Ficek Z, Gong Q H, and He Q Y 2021 *Sci. China Phys. Mech. Astron.* **64** 210311
[43] Pan J W, Simon C, Brukner Č, and Zeilinger A 2001 *Nature* **410** 212
[44] Dür W and Briegel H J 2007 *Rep. Prog. Phys.* **70** 1381
[45] Hu X M, Huang C X, Sheng Y B *et al.* 2021 *Phys. Rev. Lett.* **126** 010503
[46] Eckart S, Kunitski M, Richter M *et al.* 2018 *Nat. Phys.* **14** 701
[47] Chen Y D, Peng S N, Fu Z Y, Qiu L Y, Fan G Y, Liu Y, Wu S J, Xie X H, and Tao Z S 2024 *Commun. Phys.* **7** 98
[48] Fushitani M, Liu C N, Matsuda A *et al.* 2016 *Nat. Photonics* **10** 102
[49] Zhang Q, Xie H Q, Li G H, Wang X W, Lei H B, Zhao J, Chen Z M, Yao J P, Cheng Y, and Zhao Z X 2020 *Commun. Phys.* **3** 50
[50] Wang L, Bai G R, Wang X W *et al.* 2024 *Nat. Commun.* **15** 2705
[51] Prince K, Allaria E, Callegari C *et al.* 2016 *Nat. Photonics* **10** 176
[52] Bai Y X, Hao X L, Li W D, Yang W F, and Chen J 2023 *Phys. Rev. A* **108** 013115
[53] Lloyd S M, Babiker M, Thirunavukkarasu G, and Yuan J 2017 *Rev. Mod. Phys.* **89** 035004

[54] Blaga C I, Catoire F, Colosimo P, Paulus G, Muller H, Agostini P, and DiMauro L 2009 *Nat. Phys.* **5** 335

[55] Quan W, Lin Z, Wu M *et al.* 2009 *Phys. Rev. Lett.* **103** 093001

[56] Shafir D, Soifer H, Vozzi C, Johnson A S, Hartung A, Dube Z, Villeneuve D M, Corkum P B, Dudovich N, and Staudte A 2013 *Phys. Rev. Lett.* **111** 023005

[57] Staudte A, Ruiz C, Schöffler M, Schössler S, Zeidler D, Weber T, Meckel M, Villeneuve D M, Corkum P B, Becker A, and Dörner R 2007 *Phys. Rev. Lett.* **99** 263002

[58] Beysengulov N R, Schøyen O S, Bilek S D, Flaten J B, Leinonen O, Hjorth-Jensen M, Pollanen J, Kristiansen H E, Stewart Z J, Weidman J D, and Wilson A K 2024 *PRX Quantum* **5** 030324

[59] Liu Y Q, Tschuch S, Rudenko A, Dürr M, Siegel M, Morgner U, Moshammer R, and Ullrich J 2008 *Phys. Rev. Lett.* **101** 053001

[60] Bergues B, Kübel M, Johnson N G *et al.* 2012 *Nat. Commun.* **3** 813

[61] Kübel M, Burger C, Kling N G, Pischke T, Beaufore L, Ben-Itzhak I, Paulus G G, Ullrich J, Pfeifer T, Moshammer R, Kling M F, and Bergues B 2016 *Phys. Rev. A* **93** 053422

[62] Saitoh K, Hasegawa Y, Hirakawa K, Tanaka N, and Uchida M 2013 *Phys. Rev. Lett.* **111** 074801

[63] Tavabi A H, Rosi P, Rotunno E, Roncaglia A, Belsito L, Frabboni S, Pozzi G, Gazzadi G C, Lu P H, Nijland R, Ghosh M, Tiemeijer P, Karimi E, Dunin-Borkowski R E, and Grillo V 2021 *Phys. Rev. Lett.* **126** 094802

[64] Grillo V, Tavabi A H, Venturi F *et al.* 2017 *Nat. Commun.* **8** 15536

[65] Vidal G and Werner R F 2002 *Phys. Rev. A* **65** 032314

[66] Plenio M B 2005 *Phys. Rev. Lett.* **95** 090503

[67] Grillo V, Tavabi A H, Venturi F *et al.* 2017 *Nat. Commun.* **8** 15536

[68] Larimian S, Erattupuzha S, Baltuska A, Kitzler-Zeiler M, and Xie X H 2020 *Phys. Rev. Res.* **2** 013021

[69] Chen S, Chen J, Paulus G G, and Kang H P 2020 *Phys. Rev. A* **102** 023103